PERGAMON

Journal of Structural Geology 21 (1999) 855–874

JOURNAL OF STRUCTURAL GEOLOGY

Deformation behavior during blind thrust translation as a function of fault strength

Kevin J. Smart[a,*], Raymond D. Krieg[b], William M. Dunne[c]

[a]School of Geology and Geophysics, University of Oklahoma, Norman, OK 73019, USA
[b]Department of Civil and Environmental Engineering, University of Tennessee, Knoxville, TN 37996, USA
[c]Department of Geological Sciences, University of Tennessee, Knoxville, TN 37996, USA

Received 5 May 1998; accepted 11 February 1999

Abstract

Deformation partitioning between translation and distortion for a thrust sheet and for the roof sequence above a moving thrust horse were analyzed in terms of the role of fault strength using finite element models. Greater frictional resistance on the thrust décollement decreased fault translation, increased distortion of the thrust sheet and roof sequence, and increased the ratio of backthrusting to forethrusting for the roof sequence. In all models with weak décollements ($\mu < 0.35$), the ratio of tip-line propagation to thrust displacement is very high during initial thrust movement, but decreases significantly during later fault motion. This observation supports interpretations in natural thrust systems where thrust faults propagate large distances before accumulating significant displacements. The tip lines for weak décollements also propagated into the foreland well in advance of the distortion front in the overlying thrust sheet or roof sequence. This result does not support interpretations from natural systems for the existence of 'ductile beads' in front of propagating thrusts, but rather suggests that recent models for fault-arrest or displacement-gradient folds may be mechanically valid. In addition, no model for roof sequences yielded a simple end member response of only backthrusting or forethrusting, suggesting that the many blind thrust belts where only one response has been interpreted, may need to be re-examined. Finally, in those cases where more than one thrust flat moves simultaneously in the models, partitioning of displacement and distortion in space and time changes significantly. This result supports interpretations from natural systems where more than one thrust is thought to move at once.

1. Introduction

A fundamental aspect of thrust mechanics is the balance between fault translation and distortion of the thrusted rocks. Among the unanswered questions are: (1) what controls the partitioning between translation and distortion? and (2) how does partitioning change during the progressive development of a thrust system? For example, some workers inferred that a propagating fault-tip is preceded by a zone of distortion known as a ductile bead (e.g. Elliott, 1976; Williams and Chapman, 1983; Marshak and Engelder, 1985). This interpretation suggests that distortion is favored over translation in the early stages of thrusting. Yet, some geometric and kinematic analyses of thrust-related folds suggest that folds amplify after fault-tip propagation (e.g. Armstrong and Bartley, 1993; Wickham, 1995; Thorbjornsen and Dunne, 1997). This interpretation contrasts with the ductile bead hypothesis and suggests that initial thrusting is dominated by translation with little or no distortion. Unfortunately, these differing geometric and kinematic analyses do not allow mechanical investigations to determine the conditions necessary to trigger one type of partitioning or the other.

Partitioning between translation and distortion is further complicated by the presence of blind thrusts. Some blind thrusts separate duplex horses from an overlying roof sequence that is kinematically indepen-

* Corresponding author. Tel.: +405-325-3157; fax: +405-325-3140.
E-mail address: kjsmart@ou.edu (Kevin J. Smart)

0191-8141/99/$ - see front matter
PII: S0191-8141(99)00050-4

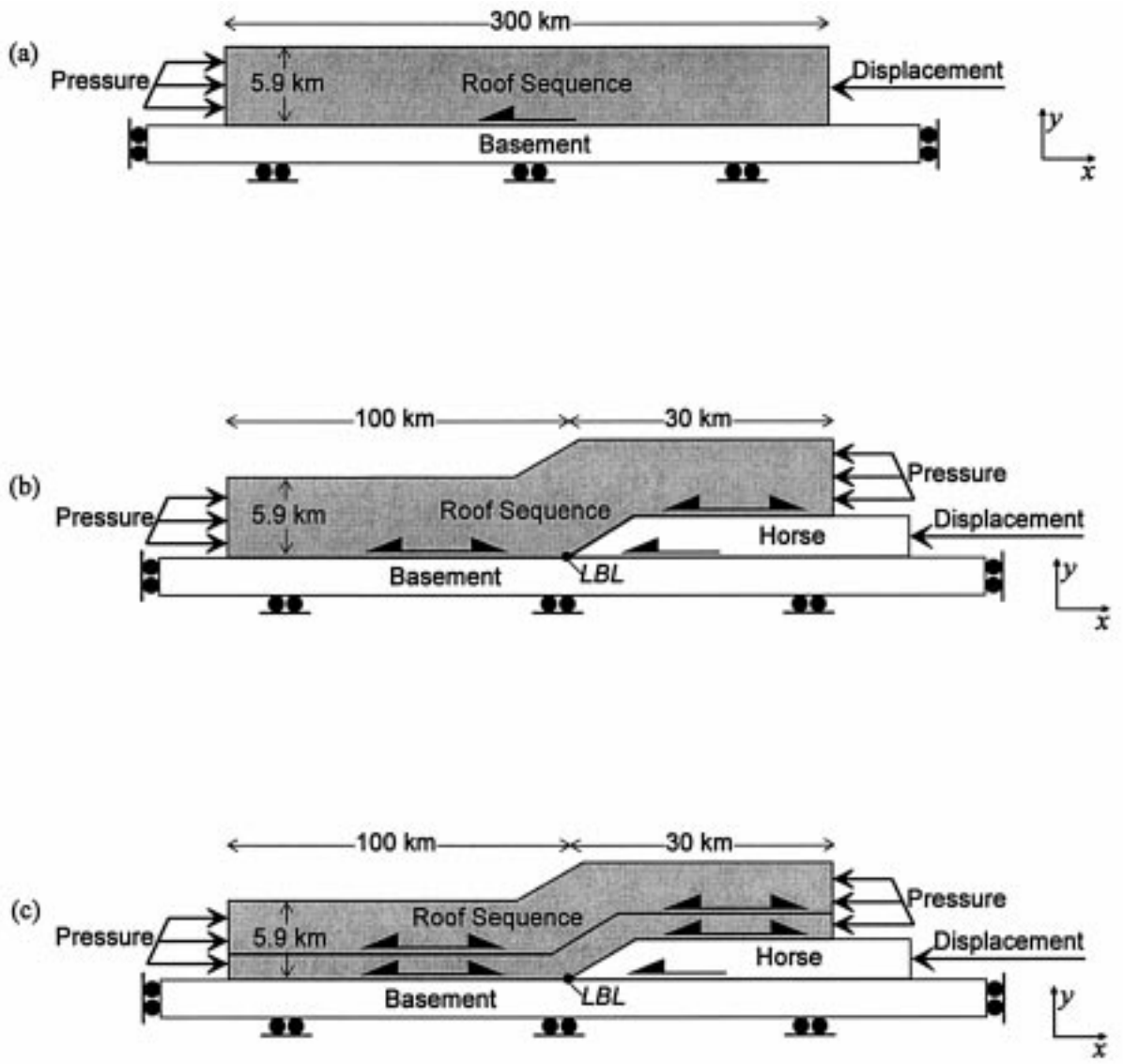

Fig. 1. Schematic illustration of finite element model initial configurations. Geometries, model dimensions, and boundary conditions for (a) thrust sheet model, and duplex models with (b) single- and (c) multiple-décollements are shown. Heavy lines indicate sliding interfaces that simulate décollement horizons where arrows show allowable slip directions. LBL is the leading branch line. The coordinate system employed in JAC2D is also shown. Note that model dimensions are given and that the figures (unlike the models) are not drawn to the same scale and have vertical exaggeration.

dent of the horses. This independence may lead to different partitioning in the roof sequence compared to a thrust sheet above a simple thrust flat. Also, more than one flat may be active in situations where thrusting is taking place on more than one thrust ramp at the same time (i.e. multiple active horses). Multiple moving thrust flats could lead to vertically stacked rock volumes with different partitioning behaviors. Since these situations are difficult to interpret from incompletely preserved final geometric and kinematic states in rocks, it is useful to simulate them to determine the mechanical controls for different partitioning behaviors.

This mechanical study uses numerical simulations to focus on the role that décollement strength plays in the balance between translation and distortion during thrusting. We construct and analyze finite element models (Fig. 1) that simulate deformation of: (1) a thrust sheet emplaced along a horizontal fault; and (2) a roof sequence during emplacement of an underlying thrust horse (duplex). These models are used to test the hypothesis that the deformation partitioning between translation and distortion in response to thrusting is strongly controlled by the fault strength. Model results will be used to address the issues of: (1) displacement accumulation as a function of fault propagation; (2) the presence or absence of a ductile bead beyond the fault tip during thrust displacement;

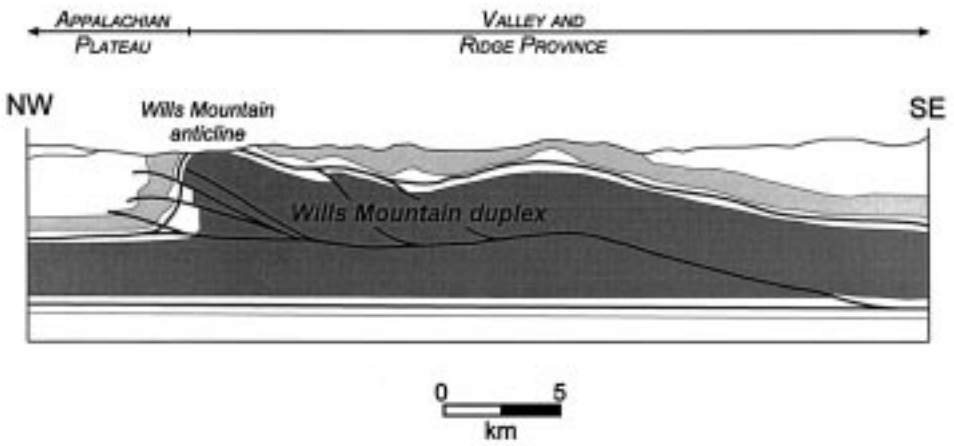

Fig. 2. Simplified geologic cross-section of the Wills Mountain duplex in the central Appalachian fold–thrust belt (modified from Wilson and Shumaker, 1988).

(3) the interaction of simultaneously moving thrust flats; and (4) the relative importance of kinematic end-member behaviors (i.e. forethrusting vs backthrusting) in a roof sequence during blind thrusting.

2. Previous modeling studies

A number of workers have published the results of numerical studies concerning aspects of thrust systems. These studies (Table A) all employed some variant of an elastic–plastic or viscous–plastic constitutive relationship to model the material behavior of the rocks in the thrust system. Generally, the choice of material parameters is similar (e.g. density, Poisson's ratio, Young's modulus), but friction magnitudes for the fault surfaces vary by nearly two orders of magnitude. This variation is significant and suggests that the strength of the décollement may play an important role in the deformational response.

While these studies examined blind thrust system geometries that are somewhat similar to our duplex models (Fig. 1), there are two key differences. Unlike our contribution, they focused on early deformation as the hanging wall begins to move up the fault ramp. As such, these models conclude at approximately the point where our duplex models begin, since our configuration assumes that the hanging wall ramp is already on the upper footwall flat. Also, these earlier models focused on hanging wall deformation in terms of distortion, and do not specifically address the interplay of both translation and distortion during thrust evolution.

3. Finite element models

Our models were constructed and analyzed with the finite element program JAC2D, a two-dimensional quasistatic nonlinear, large deformation, large strain finite element code developed at Sandia National Laboratories (Biffle and Blanford, 1994). Plane strain deformation is assumed throughout the models.

3.1. Model configurations and boundary conditions

We used models with three separate configurations to analyze roof sequence behavior during thrust movement. The simplest configuration, the 'thrust sheet' model (Fig. 1a), consists of a roof sequence above a single décollement surface. The basal surface is horizontal (i.e. no dip of basement) and there is no initial surface slope. The geometry is deformed to examine the effects of fault propagation and displacement in a thrust sheet or an overlying roof sequence without thrust imbrication underneath. This type of thrust front with a buried tip line on a thrust flat is found in thrust belts such as the central Appalachians (e.g. Wilson, 1985; Smart et al., 1997), southern Canadian Rockies (e.g. Skuce, 1996; Couzens-Schultz, 1997), and the western Urals (Brown et al., 1997).

Two more-complex models simulate the emplacement of a duplex that has a horse with a large displacement on an upper roof flat. Natural examples include the Wills Mountain duplex (Wilson and Shumaker, 1988, 1992) and North Mountain thrust sheet (Evans, 1989) in the central Appalachians, numerous horses within the southern zone of the Sulaiman fold-thrust belt of Pakistan (Jadoon et al., 1994), the Coltignone and Milan thrust duplexes in the Southern Alps of Italy (Schönborn, 1992a, b), and the Pine Pass–Peace River area of British Columbia (McMechan, 1985).

Each duplex model consists of a rigid horse and overlying roof sequence (Fig. 1b and c). Both have a décollement horizon at the base of the roof sequence.

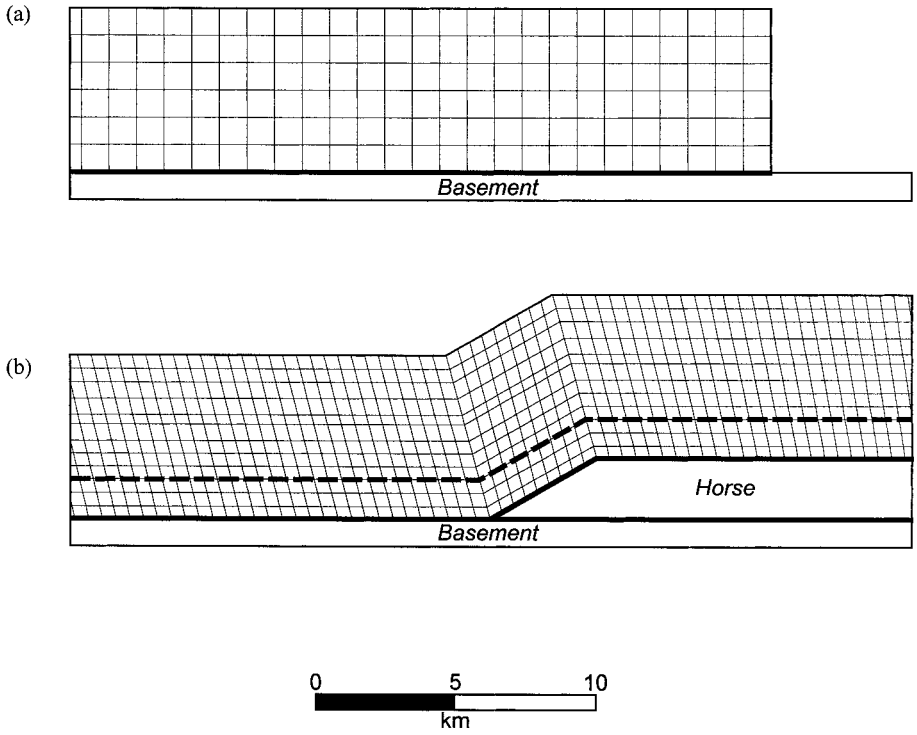

Fig. 3. Example of the undeformed finite element meshes for (a) thrust sheet and (b) duplex models. Heavy lines show locations of sliding interfaces (heavy dashed line is additional sliding interface for multiple-décollement duplex model).

The more complex models (Fig. 1c) have an additional décollement within the roof sequence that simulates a thrust system with more than one stratigraphically-weak horizon, such as the central Appalachians (Kulander and Dean, 1986; Wilson and Shumaker, 1988), the foothills of British Columbia (McMechan, 1985), and the Sulaiman fold-thrust belt of Pakistan (Jadoon et al., 1994). The multiple-décollement models also permit the issue of synchronous thrust movement (as opposed to sequential) to be addressed (Boyer, 1992).

The characteristics and geometry of these models were constructed with the leading horse and roof sequence of the Wills Mountain duplex (Fig. 2) as the template (Wilson and Shumaker, 1988, 1992; Smart, 1996; Smart et al., 1997). The thrust sheet model is 5.9 km thick, approximately the same thickness as the section of middle Ordovician and younger sedimentary

Table 1
Material parameters used in finite element models[a]

Model	Density (kg/m^3)	Young's modulus (MPa)	Poisson's ratio	Yield stress (MPa)
Thrust Sheet	2600	30 000	0.25	100
Duplex[b]				
Dunkard Grp.	2600	30 000	0.25	80
Alleghany Fm., Conemaugh and Monongahela Grps.	2600	30 000	0.25	80
Pottsville Grp.	2600	30 000	0.25	80
Greenbrier and Mauch Chunk Grps.	2600	10 000	0.25	55
Hampshire, Price, and Macrady Fms.	2550	10 000	0.20	70
Millboro Sh., Brallier Fm., and Chemung Grp.	2600	30 000	0.25	70
Juniata and Oswego Fms and Siluro-Devonian	2600	30 000	0.25	100
Martinsburg Fm.	2600	30 000	0.25	100
Cambro-Ordovician carbonates (wedge)	2700	70 000	0.35	n.a.[c]

[a] Compiled from experimental data (Jaeger and Cook, 1979; Turcotte and Schubert, 1982; Ranalli, 1987; Carmichael, 1989; Johnston and Christensen, 1992).
[b] Stratigraphic thicknesses and lithologic percentages in each unit are taken from the literature (for a summary, see Smart et al., 1997).
[c] The Cambro-Ordovician carbonates were modeled as a very strong, purely elastic material.

Table 2
Summary of finite element models

Model	Friction coefficient[a]	Maximum imposed displacement (km)	Propagation to displacement ratios				
			Tip line[b]		Plastic strain front[c]		
			Early stage[d]	Late stage[e]	Early stage[d]	Late stage[e]	Spacing between tip line and plastic strain front (km)[f]
Thrust Sheet	0.15	10	343	12	137	10	23
	0.20	10	315	9	132	7	14
	0.25	5.4	250	12	124	10	12
	0.30	1.3	196	32	107	25	9
	0.35	1.0	117	19	97	19	0
	0.40	0.8	78	11	88	16	5
Duplex (single-décollement)	0.10	10	232	6	53, 219	4, 6	20
	0.15	7.0	128	5	44, 146	3, 5	12
	0.20	7.0	78	3	24, 117	2, 4	8
	0.30	3.4	44	3	19, 98	1, 4	4
Duplex (multiple-décollement)	0.15, 0.20	3.5	133, 0	10, 7	36, 54, 109	6, 8, 11	13, 5

[a] For the multiple-décollement duplex model, values correspond to the lower and upper sliding interfaces, respectively.
[b] For the multiple-décollement duplex model, values correspond to the lower and upper sliding interfaces, respectively.
[c] For the single-décollement duplex models, values correspond to the lower (PSF1) and upper (PSF2) strain fronts, respectively. For the multiple-décollement duplex model, values correspond to the lower (PSF1), middle (PSF2), and upper (PSF3) strain fronts, respectively.
[d] 'Early Stage' corresponds to 100 m of imposed displacement.
[e] 'Late Stage' corresponds to the maximum imposed displacement for that particular model.
[f] For the single-décollement duplex models, spacing is between tip line and lower (PSF1) strain front. For the multiple-décollement duplex model, spacings are between lower tip line (TL1) and strain front (PSF1), and upper tip line (TL2) and middle strain front (PSF2), respectively.

rocks in the roof sequence that deformed during Late Paleozoic deformation. To focus on responses from changing the décollement strength rather than variations in mechanical stratigraphy, the simple thrust sheet model contained six uniform element layers (Fig. 3a) representing a thrust sheet or roof sequence with uniform material properties (Table 1). For the duplex models, the 5.9 -km-thick roof sequence was divided into eight differing element layers (Fig. 3b, Table 1) based on material properties and thicknesses of the major lithotectonic units in the Paleozoic roof sequence (Wilson and Shumaker, 1988). The 2.2 -km-thick leading horse in the duplex models represents the Cambro-Ordovician carbonates that compose the Wills Mountain duplex (Wilson and Shumaker, 1988, 1992).

The upper surface in all models is free. Fixed displacement boundary conditions are applied to the hinterland side of the roof sequence or the horse to simulate thrust displacement (Fig. 1). Gravity is imposed on each element in all models and horizontal pressure boundary conditions (Fig. 1) at exposed ends of the roof sequence replace the action of adjacent material that balances the gravitationally developed stresses and prevents spontaneous slumping. In the duplex models (Fig. 1b and c), these boundary conditions permit the roof sequence freedom to displace toward the foreland or hinterland, or to remain stationary. This freedom is particularly important because, unlike a model with a zero-displacement boundary, our simulations neither predetermine thrust tip line locations nor the kinematic response to thrusting.

Fault surfaces are modeled as sliding interfaces with simple Coulomb friction where the shear stress (product of the friction coefficient and the normal stress) on the interface must be exceeded for slip to occur (Jaeger and Cook, 1979). Preliminary models demonstrated that significant thrust displacements (i.e., greater than 3 km) required specifying friction coefficients less than about 0.35. While these values are lower than those normally reported in rock mechanics experiments (0.6–0.8) of small test specimens (e.g. Byerlee, 1967, 1978; Jaeger and Cook, 1979), the friction coefficients employed in our models represent the overall resistance to sliding and are within the range suggested by work on the strength of large faults (Turcotte and Schubert, 1982; Bird and Baumgardner, 1984; Mount and Suppe, 1987; Axen, 1992; Rice, 1992; Bird and Kong, 1994; Reiter, 1997).

Since the primary focus of this study was the role of décollement strength on the thrust sheet and roof sequence behavior, models were constructed with varying friction values (Table 2). Six variants of the thrust sheet model were analyzed by varying the coefficient of friction (μ) on the sliding interface from 0.15 to 0.40 in steps of 0.05. In these cases, a fixed displacement of 20 m per load step was applied to the right side of the roof sequence in an attempt to simulate a total of 10 km of thrust displacement (Fig. 1a).

We constructed and analyzed single-décollement duplex models with friction coefficients of 0.10, 0.15, 0.20, and 0.30 (Table 2). The horse was displaced in 10 m increments to simulate translation along the upper roof flat. As noted earlier, the pressure boundary conditions on the sides of the roof sequence balance the internal stresses developed due to gravity but do not prescribe displacement (Fig. 1b). In this way, the roof sequence responds to the developed stresses. Using the results of the single-décollement models as discussed below, our multiple-décollement model used a single configuration with friction coefficients of 0.15 for the lower and 0.20 for the upper interfaces (Table 2).

3.2. Material description

An elastic–perfectly plastic constitutive relationship based upon a pressure-independent von Mises yield condition was used to model the roof sequence rocks (Biffle and Blanford, 1994). We chose this material description, rather than a more complicated one because elastic–perfectly plastic is a good first approximation of brittle deformation in sedimentary rocks (Odé, 1960; Rudnicki and Rice, 1975; Desai and Siriwardane, 1984; Zienkiewicz and Mróz, 1984; Dougill, 1985; Davies and Fletcher, 1990). Further, experiments have demonstrated that the stress–strain relationship during low-temperature deformation of rocks is characterized by an initial elastic part followed by an inelastic (non-recoverable) portion (Jaeger and Cook, 1979; Desai and Siriwardane, 1984).

Values for the necessary constants (Table 1) were taken from the literature (Jaeger and Cook, 1979; Turcotte and Schubert, 1982; Ranalli, 1987; Carmichael, 1989; Johnston and Christensen, 1992) and are comparable to those from other numerical investigations (A). The basement in all models and the horse in the duplex models (Fig. 1) are modeled as rigid materials (Table 1). We believe this approximation is reasonable because the horse simulates the strong Cambro-Ordovician carbonates of the central Appalachians that record negligible internal deformation (Rodgers, 1963; Wiltschko and Chapple, 1977; Wilson and Shumaker, 1988).

4. Results

4.1. Thrust sheet models

The models with $\mu = 0.15$ and 0.20 achieved the desired 10 km of displacement (Table 2). Models with higher friction showed little translation of the thrust

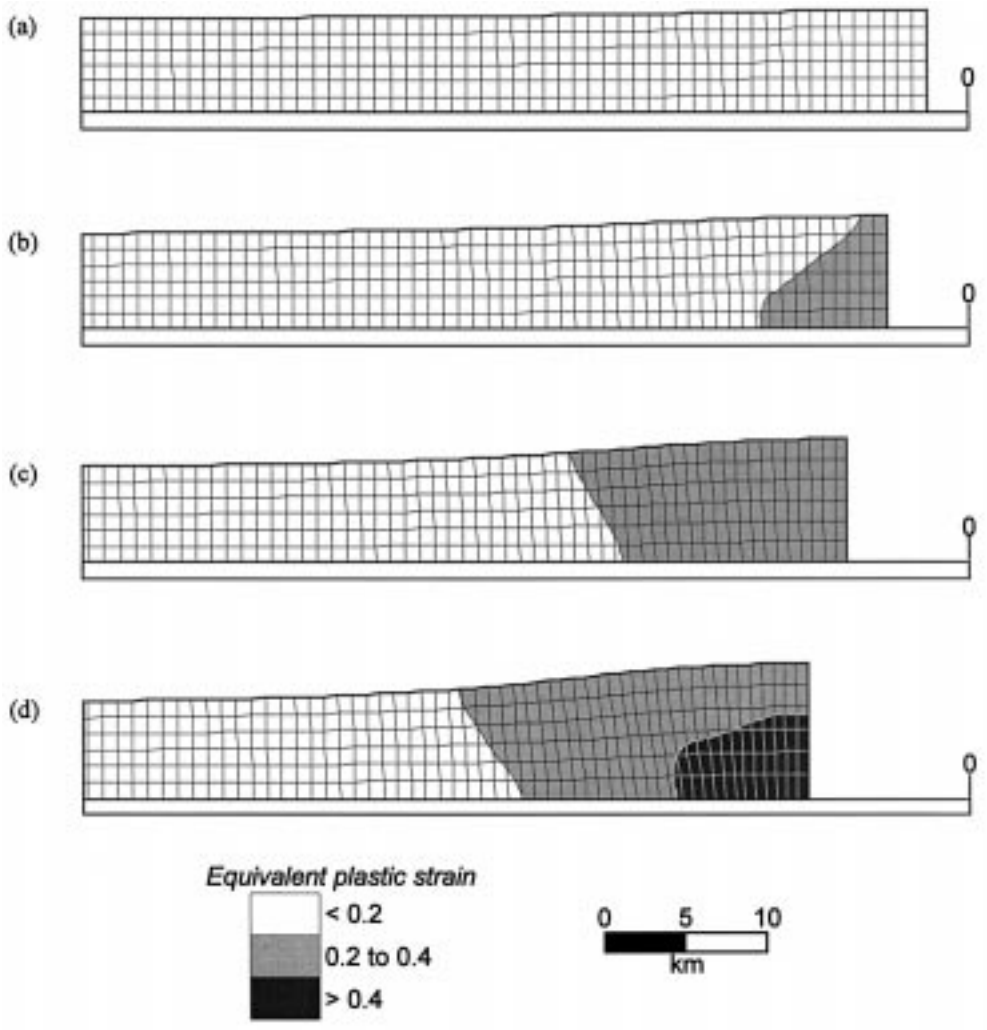

Fig. 4. Contours of equivalent plastic strain superimposed on deformed mesh for thrust sheet model with $\mu = 0.15$ after (a) 2.5 km, (b) 5 km, (c) 7.5 km, and (d) 10 km of imposed displacement.

sheet, but considerable internal shortening (distortion) adjacent to the side where the imposed displacement boundary condition was applied. Our goal was to analyze the deformation behavior related to large thrust displacements, so the small displacements of the high friction models were physically unrepresentative. In addition, the internal shortening was manifested as extreme element distortion that resulted in numerical convergence problems and extended computation times. So, the high friction models ($\mu \geq 0.25$) were not run to completion due to this unrepresentative behavior.

Contour plots of equivalent plastic strain (Hill, 1950; Malvern, 1969) superimposed on the deformed finite element mesh show the intense distortion near the right edge of the models (Figs. 4–6), producing thickening in the roof sequence. Unlike analytical solutions for a classic tapered wedge in which the entire body is yielding at an instant (Chapple, 1978; Davis et al., 1983; Dahlen et al., 1984), the roof sequence material in our models thickens by plastic deformation only after the yield stress is reached within an individual element. A flat-topped wedge or monocline grows both upward as yielding progresses and forelandward with increasing displacement (Figs. 4 and 5). Willett (1992) and Barnichon and Charlier (1996) also showed this strain concentration. Hinterland-dipping high strain shear zones develop in the monocline limb and we interpret these zones as analogs to incipient faults in nature.

The positions of two features in the models are treated as a measure of the relative role of translation vs distortion within the thrust sheet. The décollement tip line (TL) marks the furthest advance of slip on the simulated thrust flat. The leading edge of plastic deformation (plastic strain criterion $= 1 \times 10^{-6}$) at the base of the thrust sheet, referred to here as the plastic strain front (PSF), provides a measure of the foreland limit of inelastic deformation in the models. Neither the tip line nor the plastic strain front are stationary features,

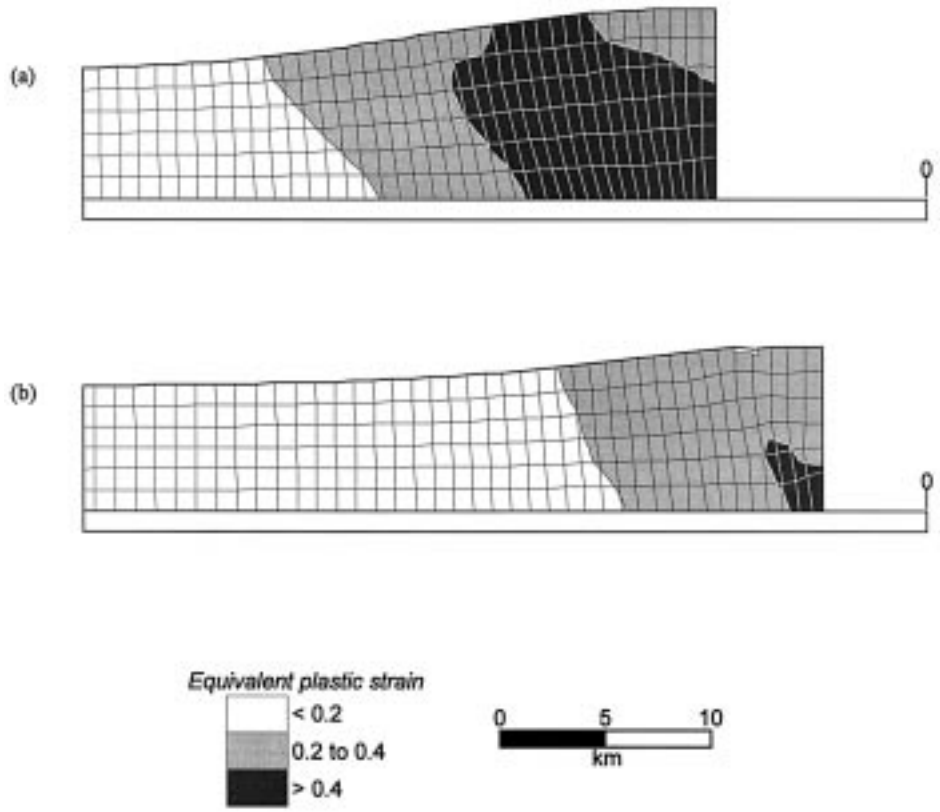

Fig. 5. Contours of equivalent plastic strain superimposed on deformed mesh for thrust sheet model with (a) $\mu = 0.20$ after 10 km and (b) $\mu = 0.25$ after 5 km of imposed displacement.

as both propagate toward the foreland with increasing thrust displacement (Fig. 8). For all friction values, the propagation to displacement ratios (PDR) are high (from 78:1 to 343:1) for initial thrusting but decrease dramatically (from 7:1 to 32:1) as maximum thrust displacement is approached (Table 2). This pattern reflects an initial period of rapid propagation relative to displacement accumulation followed by a period where propagation and displacement are nearly balanced (Fig. 8). The thrust sheet models also demonstrate that the propagation to displacement ratio decreases as the friction increases, for any thrust displacement.

For friction coefficients of 0.35 or less, the tip line PDR is higher than the plastic strain front PDR indicating that the tip line precedes the plastic strain front into the foreland (Figs. 7 and 8). The spacing between the tip line and plastic strain front is approximately constant (for a particular friction value) and does not increase or decrease as the thrust displacement increases (Fig. 8). However, the separation between the tip line and the strain front (Table 2) decreases as the friction increases from about 23 km for $\mu = 0.15$ to only 9 km for $\mu = 0.30$. With $\mu = 0.35$, the tip line and plastic strain front are virtually coincident, while in the model with $\mu = 0.40$ the plastic strain front precedes the tip line by approximately 5 km.

4.2. Duplex models with single décollement

Contours of equivalent plastic strain are superimposed on the deformed duplex models to illustrate the evolving deformation (Figs. 9 and 10). Like the thrust sheet models, greater displacement occurs on faults with smaller friction values (Table 2) and element distortion is less. The roof sequence deforms in advance of the horse by a series of low amplitude folds. These structures are clearly seen in the model with the smallest friction coefficient (compare Figs. 9 and 10). Fold amplitude decreases toward the foreland away from the leading branch line. Moderately steep (i.e., 40–50° dip) zones of high plastic strain are observed, particularly with increasing displacement (Figs. 9d and 10). Most zones dip toward the hinterland, although one foreland-dipping zone forms a conjugate pair with a hinterland-dipping zone (X in Fig. 9d).

As in the thrust sheet models, tip lines and plastic strain fronts propagate toward the foreland with increasing displacement (Fig. 11). Since the plastic strain front was not a vertical boundary (Figs. 9 and

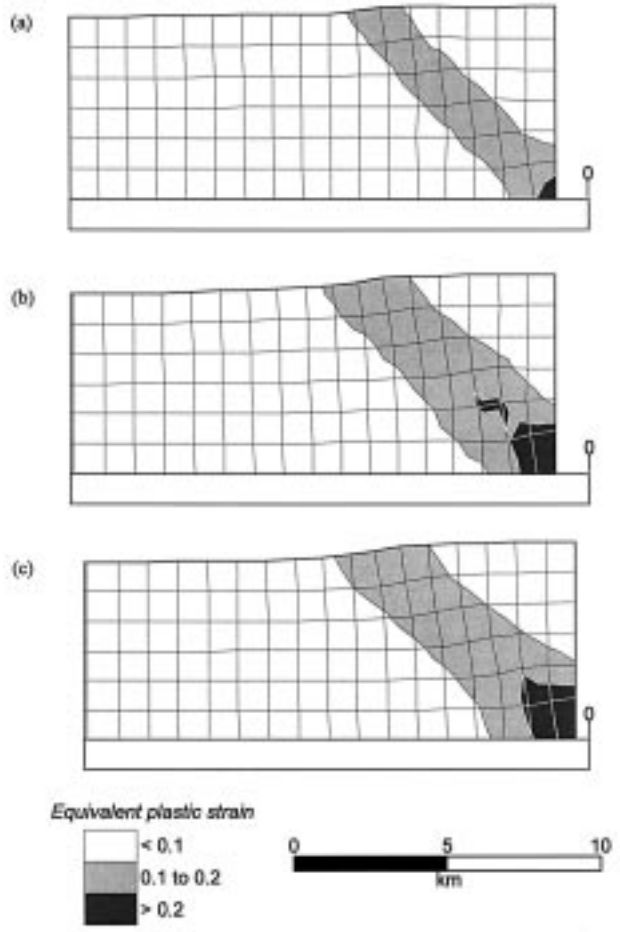

Fig. 6. Contours of equivalent plastic strain superimposed on deformed mesh for thrust sheet model with (a) $\mu = 0.30$ after 1 km, (b) $\mu = 0.35$ after 1 km, and (c) $\mu = 0.40$ after 0.8 km.

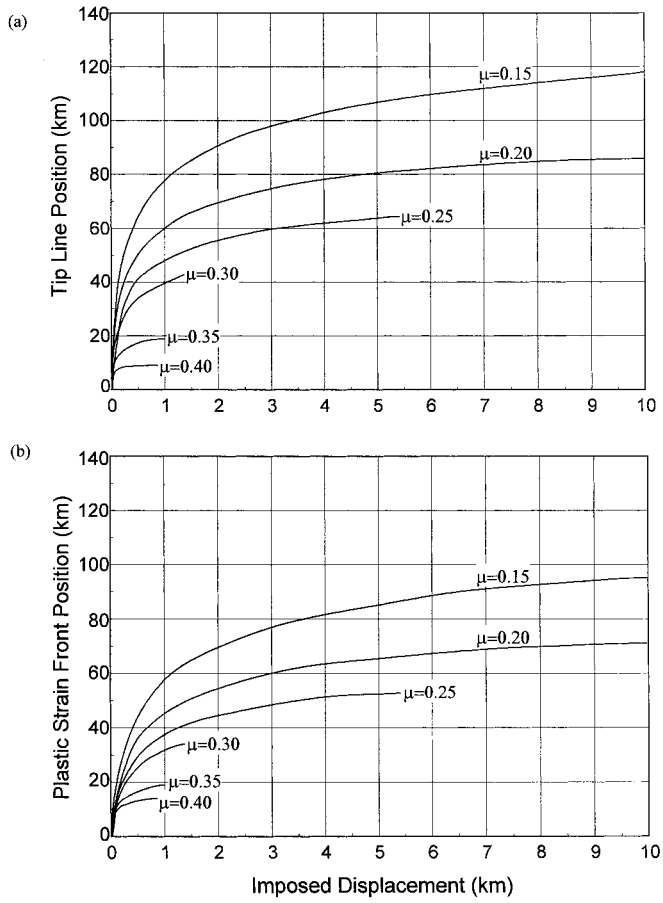

Fig. 8. (a) Tip line and (b) plastic strain front positions as a function of imposed displacement for thrust sheet models.

10), the position of the strain front was measured in two places, one adjacent to the thrust flat (labeled PSF1) and a second in the uppermost roof sequence layer (labeled PSF2). As with thrust sheet models, the propagation to displacement ratios decrease as the imposed thrust displacement increases, reaching nearly steady-state values after about 3 km of thrusting (Fig. 11, Table 2). Also similar to thrust sheet models, ratios are higher for smaller friction values. In all four models, the tip line and PSF2 precede PSF1 (Fig. 11). Yet again, the spacing between the tip line and strain front varies as a function of the friction coefficient. For $\mu = 0.10$, the tip line precedes PSF2 and is furthest (about 21 km) from PSF1. As friction increases, how-

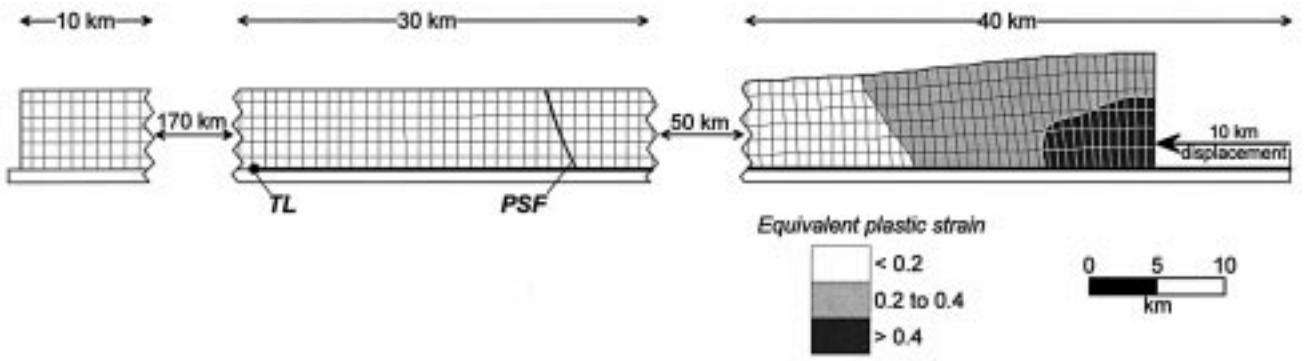

Fig. 7. Thrust sheet model ($\mu = 0.15$) after 10 km of imposed displacement showing locations of décollement tip line (TL) and plastic strain front (PSF). Contours of equivalent plastic strain are superimposed on the deformed mesh.

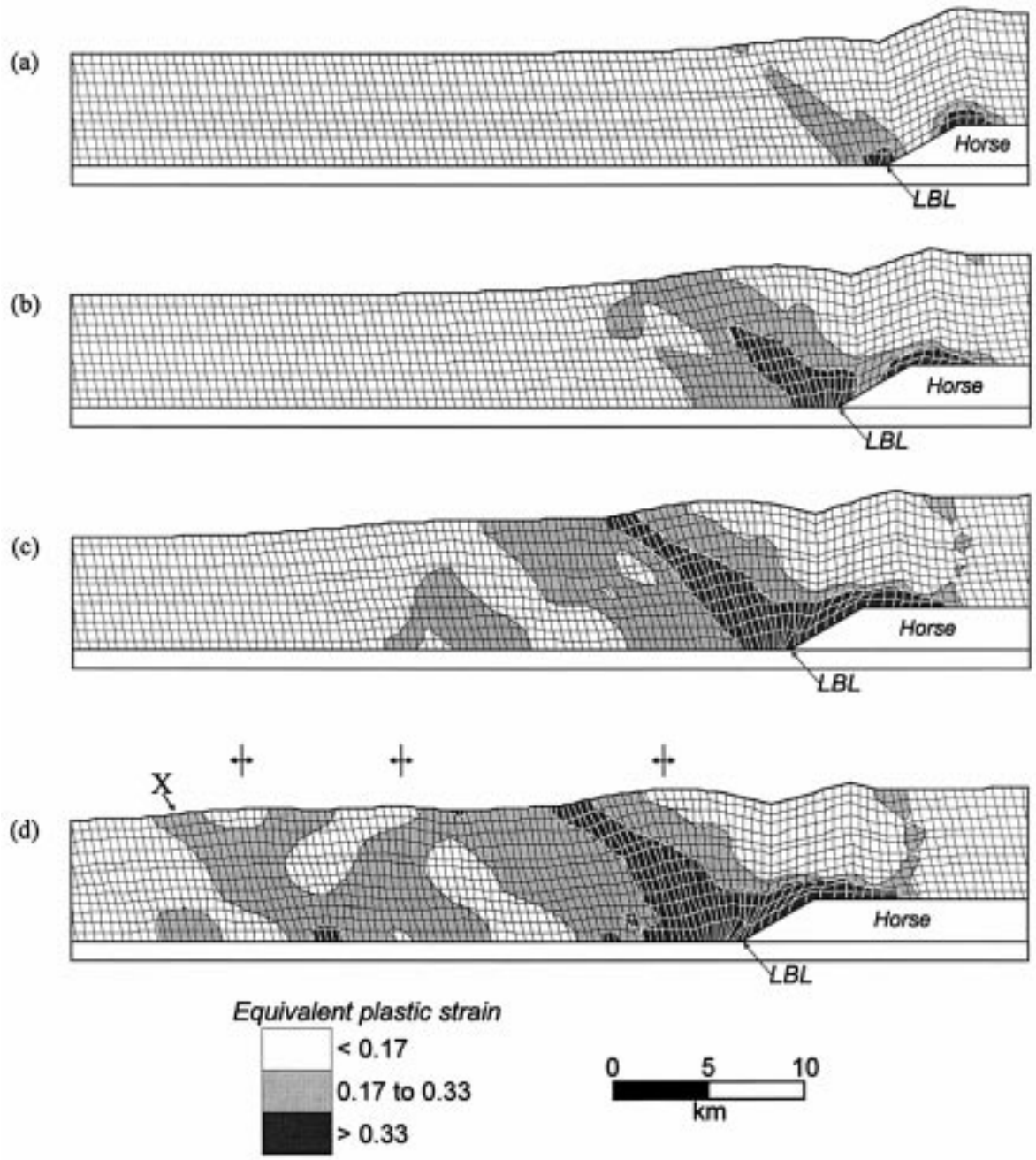

Fig. 9. Contours of equivalent plastic strain superimposed on deformed mesh for a single-décollement duplex model with $\mu = 0.10$ after (a) 2.5 km, (b) 5 km, (c) 7.5 km and (d) 10 km of imposed horse displacement. LBL is the leading branch line.

ever, two changes are observed (Fig. 11). First, the tip line and PSF2 switch relative positions such that the plastic strain front at the top of the model precedes the tip line. Second, the separation between the tip line and PSF1 decreases from approximately 20 km for $\mu = 0.10$ to only 4 km for $\mu = 0.30$ (Table 2). Again, the separation distance between tip line and strain front is dependent on friction, but independent of imposed displacement.

Unlike the thrust sheet models, the roof sequence in the duplex models is not required to translate forward (Fig. 1). Thus, displacement transfer through the leading branch line into the foreland (i.e. forethrusting) on the thrust flat may be incomplete. The roof-sequence response may accommodate this incomplete transfer by a component of backthrusting and/or local compensation. Backthrusting involves hinterland-directed transport of the roof sequence with little or no internal distortion (Banks and Warburton, 1986; Dunne and Ferrill, 1988). Local compensation requires internal

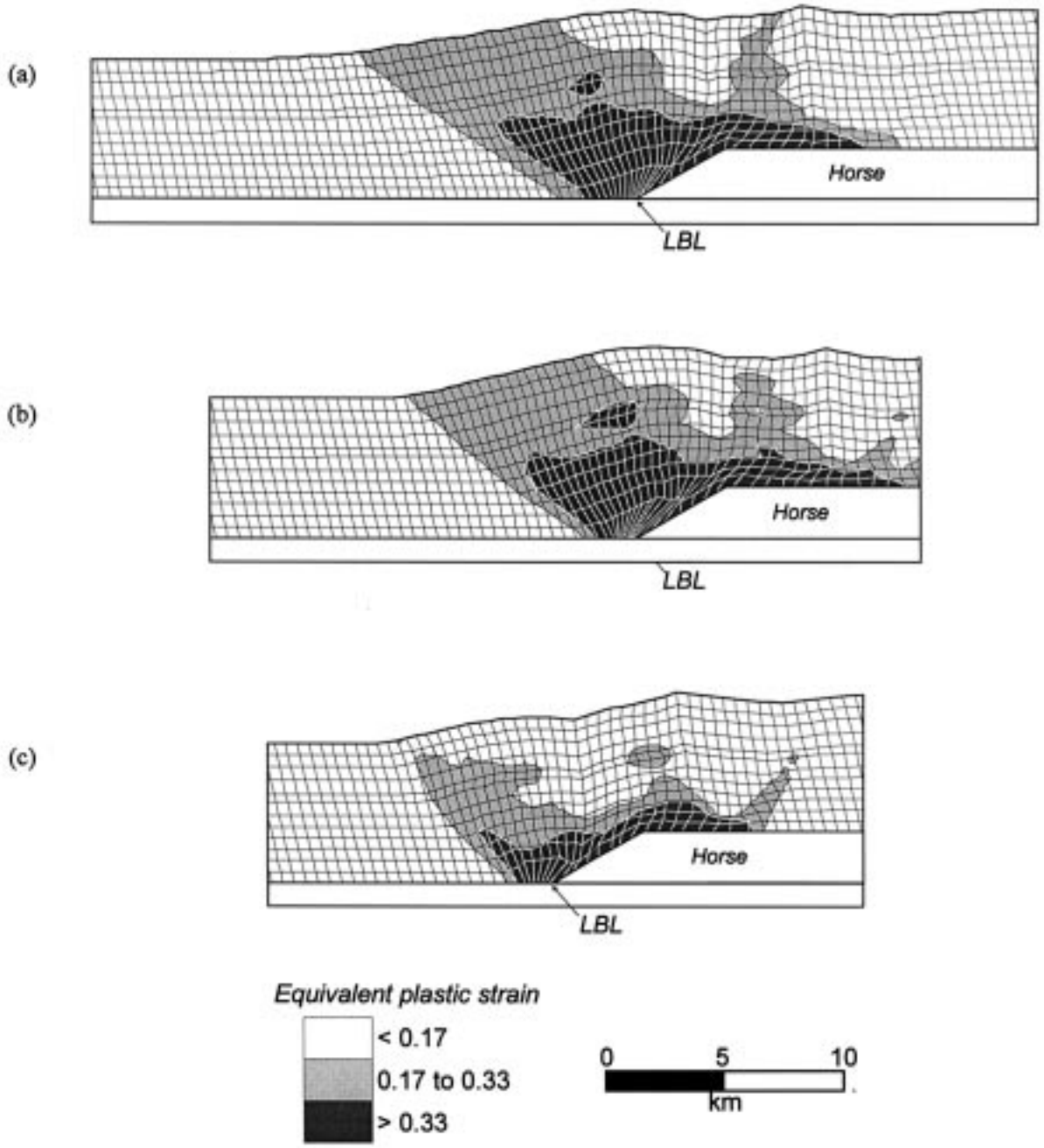

Fig. 10. Contours of equivalent plastic strain superimposed on deformed mesh for single-décollement duplex model with (a) $\mu = 0.15$ after 7 km, (b) $\mu = 0.20$ after 7 km, and (c) $\mu = 0.30$ after 3 km. LBL is the leading branch line.

thickening of the roof sequence without regional transport toward the hinterland or foreland (Ferrill and Dunne, 1989; Groshong and Epard, 1994).

In our models, the roof sequence above the horse thickens by $< 1\%$, indicating that local compensation is insignificant (Fig. 12a and b). Displacement vectors at three different levels within the roof sequence show consistent hinterland transport relative to the thrust horse (Fig. 12a and b). A component of forethrusting is present since the hinterland displacement in the roof sequence is less than the foreland displacement of the horse. Therefore, we interpret the roof sequence behavior in the single-décollement models to be a combination of forethrusting and backthrusting with negligible local compensation.

The duplex models with smaller friction coefficients show greater relative forethrusting compared to the models with larger friction values (Fig. 13). For example, for 2.5 km displacement the percentage of forethrusting increases from about 15% for $\mu = 0.30$ to

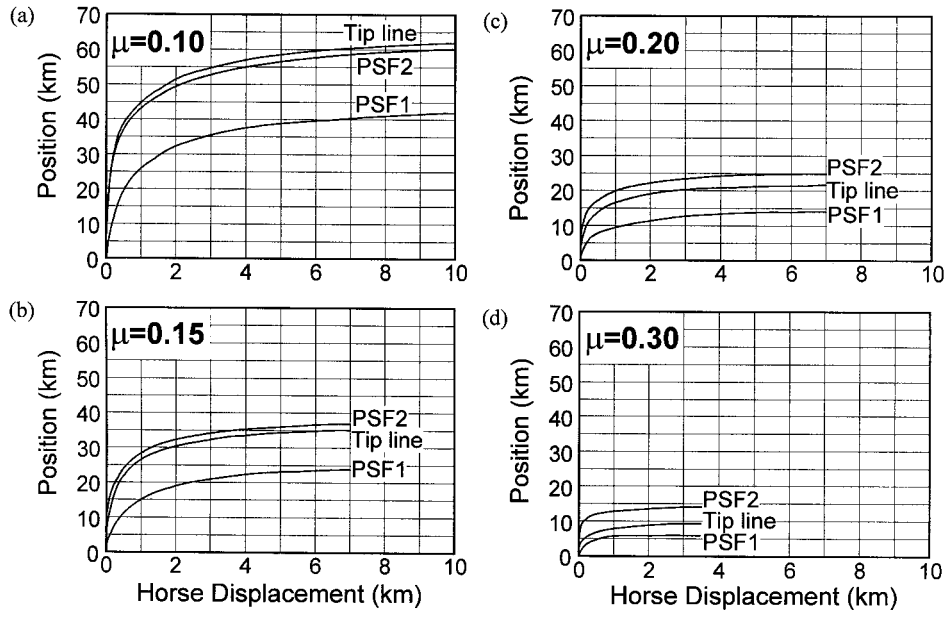

Fig. 11. Tip line and plastic strain front positions as a function of imposed horse displacement for single-décollement duplex models with friction coefficients of (a) $\mu=0.10$, (b) $\mu=0.15$, (c) $\mu=0.20$, and (d) $\mu=0.30$. PSF1 is the position of the plastic strain front adjacent to the décollement whereas PSF2 is the position of the plastic strain front in the uppermost roof sequence layer.

about 55% for $\mu=0.10$. Consequently, the percentage of backthrusting relative to forethrusting varies inversely with the magnitude of horse displacement, although all models show some plateaus in backthrusting percentage for smaller displacement values.

4.3. Duplex models with multiple décollements

Initially, both sliding interfaces in the multiple-décollement duplex model were assigned identical friction coefficients. Since slip is governed by simple

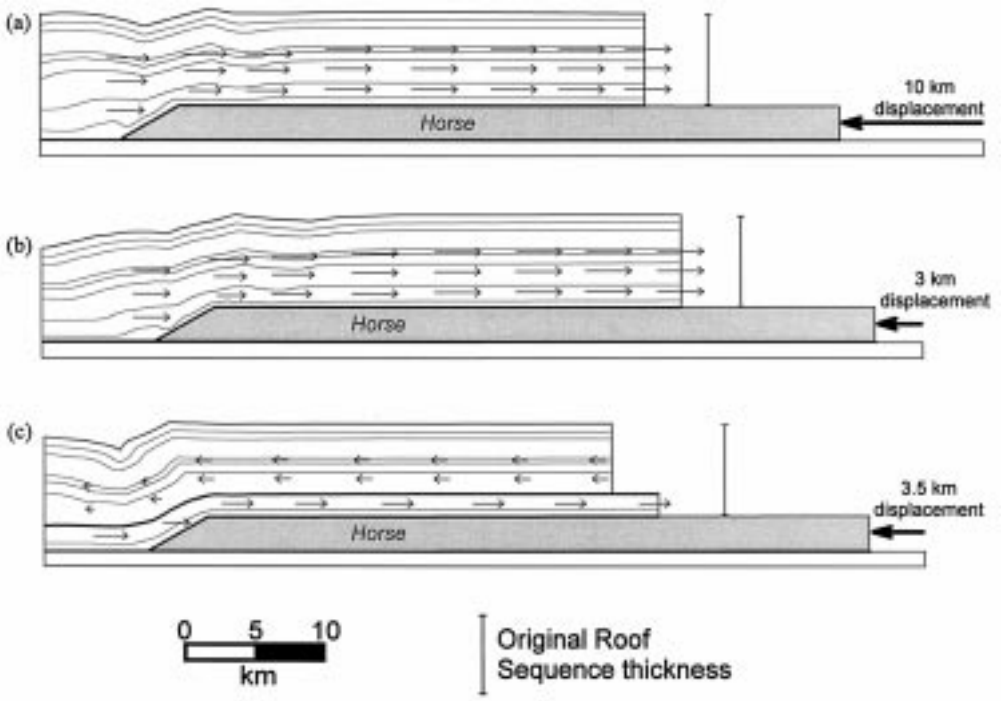

Fig. 12. Vectors of horizontal roof sequence displacement relative to the horse for single-décollement duplex models with (a) $\mu=0.10$, (b) $\mu=0.30$, and (c) multiple-décollement duplex model. Vector lengths are proportional to displacement magnitude. Original roof sequence thickness is shown for comparison to the deformed roof sequence.

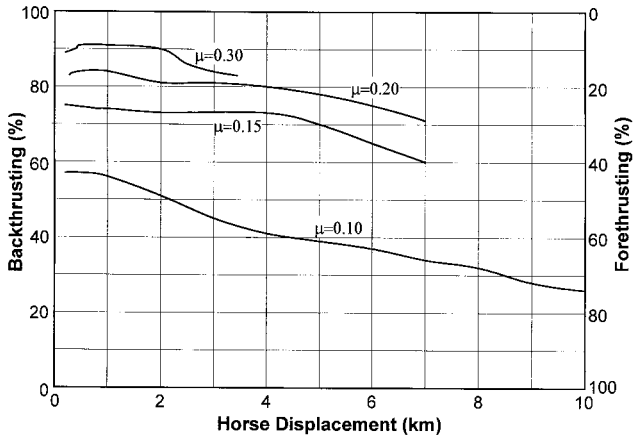

Fig. 13. Relative backthrusting–forethrusting response as a function imposed horse displacement for single-décollement duplex models of differing friction coefficients. The percentage of backthrusting and forethrusting is calculated at a node midway up on the roof sequence that is initially directly above the foreland edge of the horse.

Coulomb friction and the overburden, the upper sliding interface required less shear stress to initiate slip. Therefore, the roof sequence above the upper sliding interface underwent very little distortion but translated forward in response to the horse displacement. In contrast, the lower sliding interface remained locked such that no sliding took place. Since we were interested in analyzing roof sequence behavior with both interfaces active, we assigned a larger friction coefficient to the upper interface so that they would both slip together.

An 'equivalent friction coefficient' for each décollement was calculated such that the shear stress that must be exceeded for sliding to initiate is the same for both interfaces. The equivalent friction coefficient is given by:

$$\tau_S = \mu_L \sigma_{N_C} = \mu_U \sigma_{N_U} \quad (1)$$

where σ_N is the vertical normal stress at the lower and upper interfaces denoted by 'L' and 'U', respectively. Rearranging Eq. (1) to solve for the upper friction coefficient yields:

$$\mu_U = \frac{\mu_L \sigma_{N_L}}{\sigma_{N_U}}. \quad (2)$$

A friction coefficient for the lower interface (μ_L) of 0.15 was chosen based upon the results of the earlier thrust sheet and single-décollement models. The corresponding value of μ_U is 0.20 for the material thickness and densities employed in these simulations. As a check on Eq. (2), two additional models were analyzed with the upper interface assigned a value slightly lower (0.175) and higher (0.225) than the computed value of 0.20.

These two analyses verified the need to solve for the equivalent friction coefficient [Eq. (2)] by illustrating the sensitivity of simultaneous slip to the relative values of the friction coefficients. The first case ($\mu_L = 0.15$ and $\mu_U = 0.175$) behaved the same as the early multiple-décollement duplex model with identical friction coefficients on both interfaces. The lower interface remained locked while the upper interface slid. The second case ($\mu_L = 0.15$ and $\mu_U = 0.225$) was identical to the single-décollement duplex models because the upper interface remained locked and the lower interface slid. Consequently, only the results for the multiple-décollement model with $\mu_L = 0.15$ and $\mu_U = 0.20$ are presented.

The existence of two décollement surfaces spatially partitions the roof-sequence deformation behavior (Fig. 14). The portion of the roof sequence between the two décollements translates with relatively little distortion. A low-amplitude anticline due to distortion forms inside this portion of the roof sequence and is just in front of the leading branch line after about 2 km of imposed displacement (Fig. 14b). By 3.5 km of horse displacement, the upper sliding interface is gently folded, and an additional strain concentration develops away from the leading branch line (Fig. 14c). In contrast, the roof sequence above the upper décollement undergoes significantly greater distortion and less translation (Fig. 14). While sliding takes place on the lower décollement (TL1) when horse displacement begins, the upper interface (TL2) remains locked until 0.25 km of imposed horse displacement (Fig. 15). Once sliding occurs on the upper interface, however, the element layers in the upper part of the roof sequence begin distorting. By 1 km of imposed displacement, a low-amplitude anticline develops over the upper décollement due to distortion (Fig. 14a). This fold is centered over the tip line for the upper décollement. The fold grows both in amplitude and wavelength as the tip line propagates toward the foreland (Fig. 14b and c) and resembles a detachment fold (Jamison, 1987). Two linear high strain zones originate from the upper tip line, and dip approximately equally toward the hinterland and the foreland, respectively. They bisect the anticline limbs, but the forelimb high strain zone is considerably wider than the backlimb zone (Fig. 14c).

Just as the two portions of the roof sequence deform differently, the tip line propagation and displacement accumulation are different (Figs. 12c, 14 and 15). The propagation to displacement ratio for the lower tip line is high (133:1) for initial thrusting while the upper décollement does not move (PDR = 0) until 0.25 km of imposed displacement (Table 2, Fig. 15). As a result, the lower tip line is typically about 20 km further into the foreland than the upper tip line. Correspondingly, the lower décollement accommodates much greater relative displacement with respect to the horse and this displacement has a backthrusting sense (Fig. 12c). The upper décollement records no relative backthrusting,

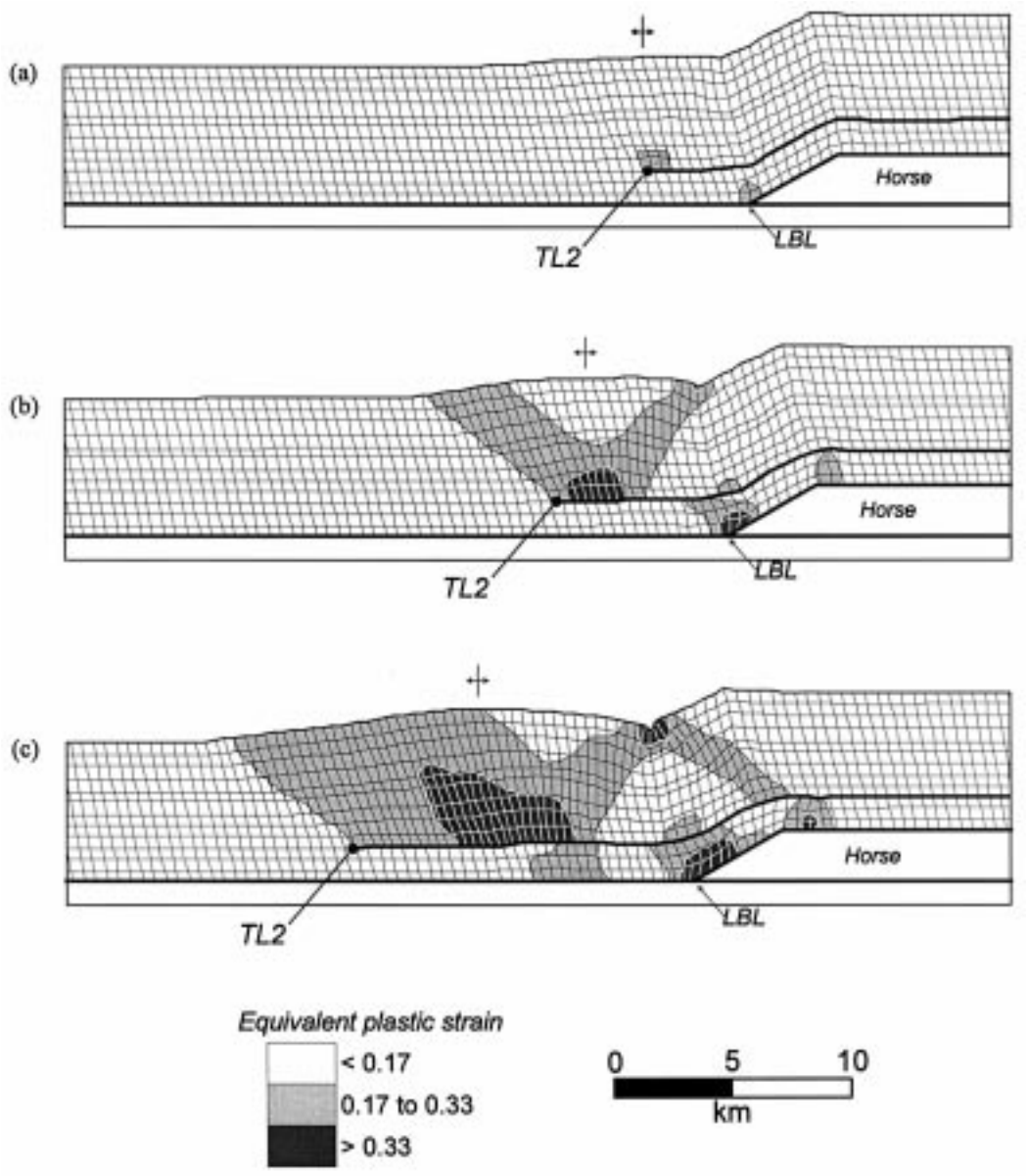

Fig. 14. Contours of equivalent plastic strain superimposed on deformed mesh for multiple-décollement duplex model with $\mu_L = 0.15$ and $\mu_U = 0.20$ after (a) 1 km, (b) 2 km, and (c) 3.5 km of imposed horse displacement. LBL is the leading branch line.

but instead forethrusting which is why the roof sequence about the upper décollement records much greater distortion than the roof sequence below this décollement (Figs. 12c and 14). These propagation patterns and displacement distributions trigger corresponding interactions between the positions of the tip lines and the plastic strain fronts. The bottom of the lower plastic strain front (PSF1, Fig. 15) trails the tip line on the lower décollement by about 13 km all through the imposed displacement. This trailing behavior is consistent with the low friction simulations for the simple duplex and thrust sheet configurations (c.f., Figs. 8 and 11). In contrast, the entire upper strain front (PSF2 and PSF3, Fig. 15) leads the tip line (TL2) of the upper décollement into the foreland, reflecting the smaller translation and greater distortion at this level of the roof sequence. Interestingly, this behavior occurs despite a relatively low friction coefficient ($\mu = 0.20$) for that décollement.

5. Discussion

5.1. Work of faulting—creation vs propagation

While these finite element models do not explicitly incorporate a term for the work necessary to create a fault surface, the slide line algorithm does address the

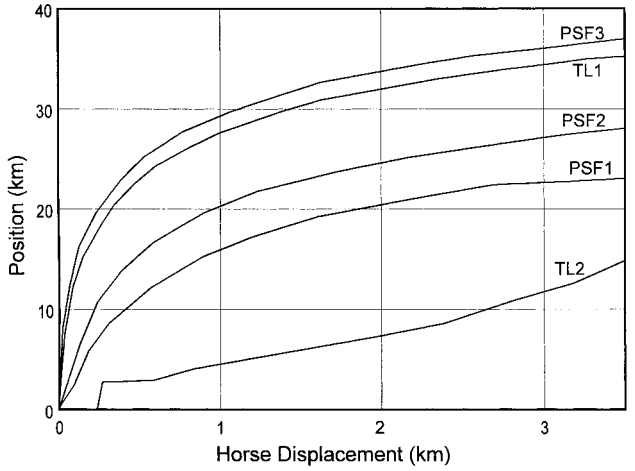

Fig. 15. Tip line and plastic strain front positions as a function of imposed horse displacement for a multiple-décollement duplex model. TL1 and TL2 are the tip lines for the lower and upper décollements, respectively. PSF1 is the position of the plastic strain front adjacent to the lower décollement, PSF2 is the position of the plastic strain front adjacent to the upper décollement, and PSF3 is the position of the plastic strain front in the uppermost roof sequence layer.

stress necessary to induce slip on an already pre-existing surface. We feel that this lack of consideration of the work of creation of the fault does not change the finite element results significantly for several reasons. First, the few studies on large faults that have addressed the work necessary to create (W_c) a fault vs the work necessary to slide (W_s) on an existing fault suggest that W_c is 2–3 orders less that W_s (Elliott, 1976; Mitra and Boyer, 1986; Williams, 1987).

Second, we suggest that greater friction values might be used as a proxy for W_c, in that greater friction would be equivalent to greater work done to create the fault and then impose translation. On this basis, should W_c be significant, then the cases with greater friction are applicable. In those cases, the plastic strain front should precede the tip line into the foreland. If W_c is not significant, then the tip line would still precede the plastic strain front for $\mu < 0.35$. Hence, while the issue of the relative importance of work done during fault surface creation is not fully resolved, we believe that the existing model results can accommodate a range of possible values for this energy term.

5.2. Strain fronts and thrust tip propagation

Since roof sequence deformation is a trade-off between translation and distortion, the evolution of the deformation can be traced by the positions of the tip lines (indicator of translation) and the plastic strain fronts (indicator of distortion). The deformation migrates progressively toward the foreland as the magnitude of thrust displacement increases (Figs. 8, 11 and 15). Propagation to displacement ratios for tip lines and plastic strain fronts are high during initial thrust displacement (Table 2). After about 1 km of displacement, however, ratios decrease sharply and eventually reach steady-state values (Table 2). For example, the thrust sheet model with $\mu = 0.15$ has an initial tip-line PDR of 343:1, which decreases to 12:1 between 5 and 10 km of thrust displacement (Fig. 8a, Table 2). This decrease is observed in all models regardless of the geometry or the friction values. This response is controlled by the rheology of the thrust sheet and its interaction with the strength of the underlying fault surface. The decrease reflects the fact that initial slip can occur on the fault surface (producing elastic strain in the overlying sheet) at stress levels below the plastic yield strength. Continued fault slip, however, requires increased stress such that the deformation becomes partitioned into both translation and plastic distortional components.

The relative positions and separation between the tip lines and plastic strain fronts are controlled entirely by the frictional resistance on the sliding interfaces and not by the displacement magnitude. In all models where $\mu < 0.35$ on a décollement, the tip line propagated in advance of the plastic strain front. The spacing between the tip line and the strain front in the thrust sheet models ranges from a maximum of 23 km for $\mu = 0.15$ to 9 km for $\mu = 0.30$ (Table 2, Fig. 8). In the single-décollement duplex models (Table 2, Fig. 11), the separation between the tip line and PSF1 ranges from 20 km with $\mu = 0.10$ down to 4 km with $\mu = 0.30$. For the multiple-décollement duplex model (Fig. 15), the tip line on the lower interface (TL1) preceded PSF1 by 13 km. The only exception is the behavior of the upper décollement in the multiple-décollement duplex model where the plastic strain front (PSF2 and PSF3) preceded the tip line (TL2) into the foreland (Fig. 15). Still, for any basal thrust with $\mu < 0.35$, the tip line precedes in advance of the plastic strain front into the foreland.

That our models show plastic strain trailing behind the thrust tip line for the basal roof thrust is intriguing because they do not show a 'ductile bead' leading the thrust into the foreland (Elliott, 1976; Williams and Chapman, 1983; Marshak and Engelder, 1985). Our results suggest that the propagation of a thrust tip will not be preceded by a zone of non-recoverable distortion (background strain of Williams and Chapman, 1983). Instead, distortion accumulates after passage of a fault tip line (e.g. Armstrong and Bartley, 1993; Wickham, 1995; Thorbjornsen and Dunne, 1997). This result may well have implications for the timing of fault-related folds and would favor displacement-gradient or fault-arrest folds over fault-propagation or some forms of break-thrust folds (Thorbjornsen and Dunne, 1997). In contrast, the plastic strain front leads the tip line on the upper décollement of the multiple-

décollement, which may mean that interplay of distortion in a thrust sheet and displacement on a thrust fault is partially a function of whether more than one fault is moving simultaneously.

5.3. Kinematic response—forethrusting vs backthrusting

All duplex models exhibit a kinematic response to duplex emplacement involving partial backthrusting of the roof sequence. The backthrusting is controlled by the frictional resistance of the décollement surface and to a lesser extent by the magnitude of thrust displacement. Lower friction values correspond to less backthrusting and more forethrusting (Fig. 13). Higher friction leads to better coupling between the horse and roof sequence in front of the leading branch line, less transfer of imposed displacement to the roof sequence, and consequently more backthrusting. For all friction values, the backthrusting–forethrusting ratio is greatest during the initial phase of horse displacement and decreases thereafter (Fig. 13). The largest decrease is observed in the model with the weakest décollement where the ratio decreases from about 1.3:1 to 0.3:1 after 10 km of thrust displacement.

While blind thrust systems are generally thought of as either forethrusting- or backthrusting-dominated (see Couzens and Wiltschko, 1996 for a recent review), the present results support a composite nature of roof sequence response to thrusting (Fig. 13). As none of the models produced an endmember response despite significant variations in décollement friction, it may be too simplistic to expect endmember behavior in any situation. Still, the relative amounts of forethrusting and backthrusting are controlled by the frictional resistance of the décollements, with weaker décollements supporting relatively more forethrusting. This result is particularly important in those studies where data are limited to the macroscale (e.g. seismic data). As an example, the absence of macroscale structures in the foreland might lead to the conclusion that backthrusting is the sole roof sequence response (e.g. the Sulaiman fold–thrust belt of Pakistan, Jadoon et al., 1994; the Andean Foothills of Argentina, Ramos, 1989). Our results suggest that such an interpretation should be resisted, particularly as forethrusting may be manifest by micro- or mesoscale structures, as in the Central Appalachians (Smart et al., 1997) or the Canadian Rockies (Couzens-Schultz, 1997). Consequently, a single endmember kinematic response should only be invoked when it can be *conclusively* demonstrated that no additional kinematic behavior is present.

5.4. Multiple roof décollements

The multiple-décollement duplex model provided several additional insights into the mechanics of roof sequence deformation during blind thrusting. The upper part of the roof sequence (i.e. material above the upper sliding interface) developed a symmetric detachment fold that grew both in amplitude and wavelength as displacement accumulated on the upper sliding interface (Fig. 14). In addition, the upper décollement, compared to the lower décollement exhibited another difference because the plastic strain front preceded the tip line. The upper décollement was the only weak ($\mu < 0.35$) one to exhibit this behavior. This décollement is different from all others because it does not connect to the décollement under the horse, so its kinematic response is not directly linked through a leading branch line. Further, it is moving simultaneously with a lower roof décollement that is directly linked to the leading branch line. As a result, much of the horse translation is partitioned to the lower roof décollement, so the upper roof sequence accommodates this blind displacement by distortion. The keys to this kinematic behavior by the upper roof sequence are the lack of direct linkage and the synchronicity of movement on two décollements, because when the higher décollement had a friction value less than the equivalent friction coefficient, it moved essentially on its own and acted like all the other weak décollements in all the other model runs.

Thus, the number of faults moving at the same time fundamentally affects the distribution of displacement and distortion in a rock mass. For vertically stacked, subhorizontal décollements, simultaneous movement may be very sensitive to the relative frictional resistances of the different slip horizons.

5.5. Friction magnitudes on large thrust flats

Roof sequence deformation in the models is partitioned between translation (fault displacement) and distortion (plastic strain). Both thrust sheet and duplex models confirm that the partitioning of deformation between distortion and translation is largely controlled by the frictional strength of the décollement surface (Figs. 4–6, 9, 10 and 14). Weak décollements favor greater roof sequence translation during blind thrusting and less internal distortion. In contrast, higher frictional resistance on the sliding interfaces leads to local distortion with very limited translation. These results support the interpretations that friction coefficients for large fault surfaces are considerably less than those predicted by measurements from small test specimens. In the context of our results, the friction values of faults with large displacements can be thought of as 'effective' friction coefficients that represent the overall resistance to sliding rather than the 'true' coefficients of friction determined in the laboratory.

5.6. Fault formation

Although the present models do not permit new faults to form automatically during a simulation, the observed zones of high plastic strain identify locations where new faults are beginning to form. These high strain zones are generally hinterland-dipping although some foreland-dipping zones develop and form crude conjugate pairs with the hinterland-dipping zones (Figs. 4–6, 9, 10 and 14). The positions and orientations of these zones are remarkably similar to the imbricate faults that develop during analogue modeling of compressive structures (e.g. Willis, 1894; Liu and Dixon, 1990, 1995; Colletta et al., 1991; Dixon and Liu, 1992; Huiqi et al., 1992; Koyi, 1995; Verschuren et al., 1996; Storti et al., 1997). Like the analogue models, the high strain zones in our models initiate near the side of the model with the imposed displacement and then form progressively further away (i.e. a foreland propagating system). The zones of high plastic strain seen in our thrust sheet models are also similar to shear zones observed in numerical models of rectangular thrust blocks by Mäkel and Walters (1993), Sassi and Faure (1996), and Barnichon and Charlier (1996). Mäkel and Walters (1993) also found that the thrust block deformation consisted of early basal slip prior to the shear zone development, just as our models produced translation prior to plastic strain.

5.7. Comparison to previous numerical models

As previously mentioned, the duplex models presented in this study share similarities and differences with several previous numerical studies (A). Most similar is model C of Erickson (1995, Fig. 3), which is based upon similar initial and boundary conditions, and a constitutive relationship. As with our study, the Erickson (1995) model developed high strain zones or shear bands in the roof sequence that identify the location of new faults. Both studies also demonstrate that in the absence of a kinematic pin, some thrust system displacement is transferred into the foreland (i.e. forethrusting). As noted earlier, our models demonstrate that greater forethrusting takes place for weaker décollements. Erickson (1995) found that backthrusting occurred only in his models where a no-displacement boundary condition (i.e. buttress or pin) was applied in the foreland to prevent forethrusting. This contrasts with our study where backthrusting occurred naturally without the constraint of a predetermined foreland pinpoint.

6. Conclusions

1. Greater frictional resistance on a blind thrust flat decreases translation, increases distortion in the overlying rocks, and increases the proportion of the backthrusting vs forethrusting for a roof sequence during displacement of a thrust horse on a roof flat.
2. The deformation, marked by both the décollement tip line and plastic strain front, propagates toward the foreland as thrust displacement increases. Propagation of the tip line is rapid for small displacements because fault slip can occur at stresses below the threshold for plastic strain. These models support interpretations for natural cases where thrust flats propagate well in advance of significant accumulations of displacement.
3. For single weak ($\mu < 0.35$) roof décollements, tip lines on the fault precede the strain front in the overlying rocks by 4–20 km. This result indicates that these thrust flats will lack ductile-bead deformation and would favor fault-related folding where the folds develop in response to displacement accumulation after thrust propagation.
4. The simultaneous movement of thrust flats significantly redistributes in space the partitioning of displacement and distortion in a roof sequence, and also the sequence in which a tip line and strain front advance into the foreland. However, simultaneous movement required that 'equivalent' friction coefficients be employed so that the overall resistance to slip be the same on each décollement.
5. No model yielded an endmember kinematic response of simple backthrusting, forethrusting, or local compensation. Instead, all models responded with a combination of forethrusting and backthrusting. As a result, unless conclusive kinematic evidence exists, endmember kinematic responses should not be interpreted to have occurred in the roof sequences of natural blind thrust belts.

Acknowledgements

Financial support was provided to K.J.S. by the Geological Society of America, the Richard C. Hasson Memorial Grant from the American Association of Petroleum Geologists, a Grant-in-Aid of Research from Sigma Xi—The Scientific Research Society, The Mayo Educational Foundation, and the Department of Geological Sciences at The University of Tennessee. Invaluable help with the finite element modeling was provided by Kevin Brown and Winston Holmes of the Department of Mechanical and Aerospace Engineering and Engineering Science at The University of Tennessee. Bill Kilsdonk, Bob Hatcher and Ken Walker are thanked for their constructive reviews during initial preparation of this manuscript. Thorough and critical reviews by JSG reviewers

Table A1
Comparison of recent numerical modelling studies of thrust systems

Author(s)	Constitutive relationship	Material parameters				Maximum displacement (m)
		Density (kg/m^3)	Elastic constants[a]	Inelastic constants[b]	Fault surface[c]	
Current study	Elastic–perfectly plastic	2550–2700	$E = 10\,000$–$30\,000$ $\nu = 0.20$–0.35	$\sigma_y = 55$–100	$\mu = 0.10$–0.40	10 000
Strayer and Huddleston (1997)	Elastic–perfectly plastic	2600–2690	$E = 11\,093$–$28\,615$[d] $\nu = 0.30$[d]	$\alpha = 14$–$42°$ $C_o = 6.72$–38.4	$\mu = 0.02$–0.09 $\lambda_N = 10^{11}$; $\lambda_S = 10^{11}$	4.5[e]
Jamison (1996)	Viscous–plastic	unspecified	unspecified	$\alpha = 21.8°$; $C_o = 20$–40 $\eta = 1 \times 10^{15}$	$\mu = 0.05$–0.45	4000
Erickson and Jamison (1995)	Viscous–plastic	2500	$E = 30\,000$ $\nu = 0.25$; $\beta = 0.2$	$\sigma_y = 10$–31; $H = 60$–2300 $\eta = 1.5$–5.0×10^{15}	$\mu = 0.01$	2500
Erickson (1995)	Elastic–plastic	2500	$E = 30\,000$ $\nu = 0.25$; $\beta = 0.2$	$\sigma_y = 3.5$–31.2 $H = 60$–2300	$\mu = 0.01$–0.6	2000

[a] Abbreviations: E—Young's modulus (MPa); ν—Poisson's ratio; β—Pressure-dependence coefficient.
[b] Abbreviations: σ_y—Plastic yield stress (MPa); α—Friction angle; C_o—Cohesion (MPa); η—Viscosity (MPa-s); H—Plastic hardening modulus (MPa).
[c] Abbreviations: μ—Friction coefficient; λ_N—Normal stiffness (Pa/m); λ_S—Shear stiffness (Pa/m).
[d] Paper reports bulk and shear moduli rather than Young's modulus and Poisson's ratio.
[e] Models simulated mesoscale features so displacements are considerably smaller than other studies.

William Jamison and Dave Wiltschko, and JSG editor Donald Fisher significantly improved the final product.

References

Armstrong, P.A., Bartley, J.M., 1993. Displacement and deformation associated with a lateral thrust termination, southern Golden Gate Range, southern Nevada, U.S.A. Journal of Structural Geology 15, 721–735.

Axen, G.J., 1992. Pore pressure, stress increase, and fault weakening in low-angle normal faulting. Journal of Geophysical Research 97, 8979–8991.

Banks, C.J., Warburton, J., 1986. 'Passive-roof' duplex geometry in the frontal structures of the Kirthar and Sulaiman mountain belts, Pakistan. Journal of Structural Geology 8, 229–237.

Barnichon, J.D., Charlier, R., 1996. Finite element modelling of the competition between shear bands in the early stages of thrusting: Strain localization analysis and constitutive law influence. In: Buchanan, P.G., Nieuwland, D.A. (Eds.), Modern Developments in Structural Interpretation, Validation and Modeling, 99. Geological Society Special Publication, pp. 235–250.

Biffle, J.H., Blanford, M.L., 1994. JAC2D—a two-dimensional finite element computer program for the nonlinear quasi-static response of solids with the conjugate gradient method. Sandia National Laboratory Report SAND93–1891.

Bird, P., Baumgardner, J., 1984. Fault friction, regional stress, and crust–mantle coupling in southern California from finite element models. Journal of Geophysical Research 89, 1932–1944.

Bird, P., Kong, X., 1994. Computer simulations of California tectonics confirm very low strength of major faults. Geological Society of America Bulletin 106, 159–174.

Boyer, S.E., 1992. Geometric evidence for synchronous thrusting in the southern Alberta and northwest Montana thrust belts. In: McClay, K.R. (Ed.), Thrust Tectonics. Chapman and Hall, London, pp. 377–390.

Brown, D., Alvarez-Marrón, J., Pérez-Estaún, A., Gorozhanina, Y., Baryshev, V., Puchkov, V., 1997. Geometric and kinematic evolution of the foreland thrust and fold belt in the southern Urals. Tectonics 16, 551–562.

Byerlee, J.D., 1967. Theory of friction based on brittle fracture. Journal of Applied Physics 38, 2928–2934.

Byerlee, J.D., 1978. Friction of Rocks. Pure and Applied Geophysics 116, 615–626.

Carmichael, R.S., 1989. Practical Handbook of Physical Properties of Rocks and Minerals. CRC Press, Boca Raton.

Chapple, W.M., 1978. Mechanics of thin-skinned fold-and-thrust belts. Geological Society of America Bulletin 89, 1189–1198.

Colletta, B., Letouzey, J., Pinedo, R., Ballard, J.F., Balé, P., 1991. Computerized X-ray tomography analysis of sandbox models: examples of thin-skinned thrust systems. Geology 19, 1063–1067.

Couzens-Schultz, B.A., 1997. The effects of mechanical stratigraphy on the origin of triangle zones in thrust belts. Unpublished Ph.D. thesis. Texas A & M University, College Station, U.S.A.

Couzens, B.A., Wiltschko, D.V., 1996. The control of mechanical stratigraphy on the formation of triangle zones. Canadian Petroleum Geology bulletin 44, 165–179.

Dahlen, F.A., Suppe, J., Davis, D., 1984. Mechanics of fold-and-thrust belts and accretionary wedges: cohesive Coulomb theory. Journal of Geophysical Research 89, 10087–10101.

Davies, R.K., Fletcher, R.C., 1990. Shear bands in a plastic layer at yield under combined shortening and shear: a model for the fault array in a duplex, Knipe, R.J., Rutter, E.H. (Eds.), Deformation

Mechanisms, Rheology and Tectonics. Geological Society of London Special Publication, 54, pp. 123–131.
Davis, D., Suppe, J., Dahlen, F.A., 1983. Mechanics of fold-and-thrust belts and accretionary wedges. Journal of Geophysical Research 88, 1153–1172.
Desai, C.S., Siriwardane, H.J., 1984. Constitutive Laws for Engineering Materials with Emphasis on Geologic Materials. Prentice-Hall, Engelwood Cliffs.
Dixon, J.M., Liu, S., 1992. Centrifuge modelling of the propagation of thrust faults. In: McClay, K.R. (Ed.), Thrust Tectonics. Chapman and Hall, London, pp. 53–69.
Dougill, J.W., 1985. Constitutive relations for concrete and rock: Applications and extensions of elasticity and plasticity theory. In: Bazant, Z.P. (Ed.), Mechanics of Geomaterials. Rocks, Concretes, Soils. John Wiley and Sons Ltd, Chichester, pp. 21–46.
Dunne, W.M., Ferrill, D.A., 1988. Blind thrust systems. Geology 16, 33–36.
Elliott, D., 1976. The energy balance and deformation mechanisms of thrust sheets. Philosophical Transactions of the Royal Society of London 283, 289–312.
Erickson, S.G., 1995. Mechanics of triangle zones and passive-roof duplexes: Implications of finite-element models. Tectonophysics 245, 1–11.
Erickson, S.G., Jamison, W.R., 1995. Viscous–plastic finite-element models of fault-bend folds. Journal of Structural Geology 17, 561–573.
Evans, M.A., 1989. The structural geometry and evolution of foreland thrust systems, northern Virginia. Geological Society of America Bulletin 101, 339–354.
Ferrill, D.A., Dunne, W.M., 1989. Cover deformation above a blind duplex: An example from West Virginia, U.S.A. Journal of Structural Geology 11, 421–431.
Groshong Jr., R.H., Epard, J.-L., 1994. The role of strain in area-constant detachment folding. Journal of Structural Geology 16, 613–618.
Hill, R., 1950. The Mathematical Theory of Plasticity. Oxford University Press, London.
Huiqi, L., McClay, K.R., Powell, D., 1992. Physical models of thrust wedges. In: McClay, K.R. (Ed.), Thrust Tectonics. Chapman and Hall, London, pp. 71–81.
Jadoon, I.A.K., Lawrence, R.D., Lillie, R.J., 1994. Seismic data, geometry, evolution, and shortening in the active Sulaiman fold-and-thrust belt of Pakistan, southwest of the Himalayas. American Association of Petroleum Geologists bulletin 78, 758–774.
Jaeger, J.C., Cook, W., 1979. Fundamentals of Rock Mechanics. Chapman and Hall, London.
Jamison, W.R., 1987. Geometric analysis of fold development in overthrust terranes. Journal of Structural Geology 9, 207–219.
Jamison, W.R., 1996. Mechanical models of triangle zones. Bulletin of Canadian Petroleum Geology 44, 180–194.
Johnston, J.E., Christensen, N.I., 1992. Shear wave reflectivity, anisotropies, Poisson's ratios, and densities of a southern Appalachian Paleozoic sedimentary sequence. Tectonophysics 210, 1–20.
Koyi, H., 1995. Mode of internal deformation in sand wedges. Journal of Structural Geology 17, 293–300.
Kulander, B.R., Dean, S.L., 1986. Structure and tectonics of central and southern Appalachian Valley and Ridge and Plateau Provinces, West Virginia and Virginia. American Association of Petroleum Geologists bulletin 70, 1674–1684.
Liu, S., Dixon, J.M., 1990. Centrifuge modeling of thrust faulting: strain partitioning and sequence of thrusting in duplex structures, Knipe, R.J., Rutter, E.H. (Eds.), Deformation Mechanisms, Rheology and Tectonics. Geological Society of London Special Publication, 54, pp. 431–444.
Liu, S., Dixon, J.M., 1995. Localization of duplex thrust-ramps by buckling: analog and numerical modelling. Journal of Structural Geology 17, 875–886.
Mäkel, G., Walters, J., 1993. Finite-element analyses of thrust tectonics: computer simulation of detachment phase and development of thrust faults. Tectonophysics 226, 167–185.
Malvern, L.E., 1969. Introduction to the Mechanics of a Continuous Medium. Prentice-Hall, Inc, New Jersey.
Marshak, S., Engelder, T., 1985. Development of cleavage in a fold-thrust belt in eastern New York. Journal of Structural Geology 7, 345–359.
McMechan, M.E., 1985. Low-taper triangle-zone geometry: an interpretation for the Rocky Mountain foothills, Pine Pass–Peace River area, British Columbia. Canadian Petroleum Geology bulletin 33, 31–38.
Mitra, G., Boyer, S.E., 1986. Energy balance and deformation mechanisms of duplexes. Journal of Structural Geology 8, 291–304.
Mount, V.S., Suppe, J., 1987. State of stress near the San Andreas fault: Implications for wrench tectonics. Geology 15, 1143–1146.
Odé, H., Geological Society of America Memoir, 1960. Faulting as a velocity discontinuity in plastic deformation. In: Griggs, D., Handin, J. (Eds.), Rock Deformation (A Symposium), 79, pp. 293–321.
Ramos, V.A., 1989. Andean foothills structures in Northern Magallanes Basin, Argentina. American Association of Petroleum Geologists bulletin 73, 887–903.
Ranalli, G., 1987. Rheology of the Earth: Deformation and Flow Processes in Geophysics and Geodynamics. Allen and Unwin Inc, Boston.
Reiter, M., 1997. A note comparing parameters controlling low-angle normal and thrust movement. Journal of Structural Geology 19, 99–106.
Rice, J.R., 1992. Fault stress states, pore pressure distributions, and the weakness of the San Andreas Fault. In: Evans, B., Wong, T.F. (Eds.), Fault Mechanics and Transport Properties of Rocks. Academic Press, San Diego, pp. 475–504.
Rodgers, J., 1963. Mechanics of Appalachian foreland folding in Pennsylvania and West Virginia. American Association of Petroleum Geologists bulletin 47, 1527–1536.
Rudnicki, J.W., Rice, J.R., 1975. Conditions for localization of deformation in pressure-sensitive materials. Journal of the Mechanics and Physics of Solids 23, 371–394.
Sassi, W., Faure, J.-L., 1996. Role of faults and layer interfaces on the spatial variation of stress regimes in basins: inferences from numerical modelling. Tectonophysics 266, 101–119.
Schönborn, G., 1992a. Kinematics of a transverse zone in the Southern Alps, Italy. In: McClay, K.R. (Ed.), Thrust Tectonics. Chapman and Hall, London, pp. 299–310.
Schönborn, G., 1992b. Alpine tectonics and kinematic models of the Central Southern Alps. Memorie Di Scienze Geologiche XLIV, 229–393.
Skuce, A.G., 1996. Frontal Foothills structures in central Alberta: the thin end of the intercutaneous wedge? Canadian Petroleum Geology bulletin 44, 153–164.
Smart, K.J., 1996. Kinematic analysis and mechanical modeling of roof sequence response to blind thrusting. Unpublished Ph.D. thesis. University of Tennessee, Knoxville, U.S.A.
Smart, K.J., Dunne, W.M., Krieg, R.D., 1997. Roof sequence response to emplacement of the Wills Mountain blind duplex: The roles of forethrusting and scales of deformation. Journal of Structural Geology 19, 1443–1459.
Storti, F., Salvini, F., McClay, K., 1997. Fault-related folding in sandbox analogue models of thrust wedges. Journal of Structural Geology 19, 583–602.
Strayer, L.M., Huddleston, P.J., 1997. Numerical modeling of fold initiation at thrust ramps. Journal of Structural Geology 19, 551–566.
Thorbjornsen, K.L., Dunne, W.M., 1997. Origin of a thrust-related

fold: geometric vs kinematic tests. Journal of Structural Geology 19, 303–319.

Turcotte, D.L., Schubert, G., 1982. Geodynamics: Applications of Continuum Physics to Geological Problems. John Wiley and Sons, Inc, New York.

Verschuren, M., Nieuwland, D., Gast, J., 1996. Multiple detachment levels in thrust tectonics: sandbox experiments and palinspastic reconstructions. In: Buchanan, P.G., Nieuwland, D.A. (Eds.), Modern Developments in Structural Interpretation, Validation and Modeling, 99. Geological Society Special Publication, pp. 227–234.

Wickham, J., 1995. Fault displacement-gradient folds and the structure at Lost Hills, California (U.S.A.). Journal of Structural Geology 17, 1293–1302.

Willett, S.D., 1992. Dynamic and kinematic growth and change of a Coulomb wedge. In: McClay, K.R. (Ed.), Thrust Tectonics. Chapman and Hall, London, pp. 19–31.

Williams, R.T., 1987. Energy balance for large thrust sheets and fault-bend folds. Journal of Structural Geology 9, 375–379.

Williams, G., Chapman, T., 1983. Strains developed in the hanging walls of thrust due to their slip/propagation rate: a dislocation model. Journal of Structural Geology 5, 563–571.

Willis, B., 1894. The mechanics of Appalachian structure. United States Geological Survey 13th Annual Report 1891–1892, Part 2. 211–282.

Wilson, T.H., 1985. Section 11. In: Woodward, N.B. (Eds.), Valley and Ridge Thrust Belt: Balanced Structural Sections, Pennsylvania to Alabama. University of Tennessee Department of Geological Sciences Studies in Geology, 12, pp. 30–31.

Wilson, T.H., Shumaker, R.C., 1988. Three-dimensional structural interrelationships within Cambrian–Ordovician lithotectonic unit of central Appalachians. American Association of Petroleum Geologists bulletin 72, 600–614.

Wilson, T.H., Shumaker, R.C., 1992. Broad Top thrust sheet: an extensive blind thrust in the central Appalachians. American Association of Petroleum Geologists bulletin 76, 1310–1324.

Wiltschko, D.V., Chapple, W.M., 1977. Flow of weak rocks in Appalachian Plateau folds. American Association of Petroleum Geologists bulletin 61, 653–670.

Zienkiewicz, O.C., Mróz, Z., 1984. Generalized plasticity formulation and applications to geomechanics. In: Desai, C.S., Gallagher, R.H. (Eds.), Mechanics of Engineering Materials. John Wiley and Sons, Ltd, Chichester, pp. 655–679.